Identification of Nicotinic Acetylcholine Receptor Amino Acids Photolabeled by the Volatile Anesthetic Halothane†

David C. Chiara,‡ Lawrence J. Dangott,‡,§ Roderic G. Eckenhoff,*,|| and Jonathan B. Cohen*,‡

Department of Neurobiology, Harvard Medical School, Boston, Massachusetts 02115, and Department of Anesthesia, University of Pennsylvania, Philadelphia, Pennsylvania 19104

Received July 3, 2003; Revised Manuscript Received September 12, 2003

ABSTRACT: To identify inhalational anesthetic binding domains in a ligand-gated ion channel, we photolabeled nicotinic acetylcholine receptor (nAChR)-rich membranes from *Torpedo* electric organ with [^{14}C]halothane and determined by Edman degradation some of the photolabeled amino acids in nAChR subunit fragments isolated by sodium dodecyl sulfate−polyacrylamide gel electrophoresis and high-performance liquid chromatography. Irradiation at 254 nm for 60 s in the presence of 1 mM [^{14}C]halothane resulted in incorporation of ∼0.5 mol of ^{14}C/mol of subunit, with photolabeling distributed within the nAChR extracellular and transmembrane domains, primarily at tyrosines. γTyr-111 in ACh binding site segment E was labeled, while αTyr-93 in segment A was not. Within the transmembrane domain, αTyr-213 within αM1 and δTyr-228 within δM1 were photolabeled, while no labeled amino acids were identified within the δM2 ion channel domain. Although the efficiency of photolabeling at the subunit level was unaffected by agonist, competitive antagonist, or isoflurane, state-dependent photolabeling was seen in a δ subunit fragment beginning at δPhe-206. Labeling of δTyr-212 in the extracellular domain was inhibited >90% by *d*-tubocurarine, whereas addition of either carbamylcholine or isoflurane had no effect. Within M1, the level of photolabeling of δTyr-228 with [^{14}C]halothane was increased by carbamylcholine (90%) or *d*-tubocurarine (50%), but it was inhibited by isoflurane (40%). Within the structure of the nAChR transmembrane domain, δTyr-228 projects into an extracellular, water accessible pocket formed by amino acids from the δM1−δM3 α-helices. Halothane photolabeling of δTyr-228 provides initial evidence that halothane and isoflurane bind within this pocket with occupancy or access increased in the nAChR desensitized state compared to the closed channel state. Halothane binding at this site may contribute to the functional inhibition of nAChRs.

At clinically effective concentrations, most general anesthetics modulate the function of ligand-gated ion channels in the superfamily that includes nicotinic acetylcholine receptors (nAChRs)[1] and serotonin 5-HT$_3$ receptors with cation-selective channels, as well as the GABA$_A$ receptors and glycine receptors with anion-selective channels (*1*−*3*). General anesthetics enhance agonist action for most of the receptors with anion-selective channels, while they inhibit noncompetitively nAChRs. Members of this superfamily are composed of five homologous subunits arranged pseudo-symmetrically about a central axis that is the ion channel. Each subunit has a large N-terminal segment that contributes to the receptor extracellular domain and four transmembrane segments (M1−M4). The agonist binding sites are contained in the extracellular domain at subunit interfaces. The M2 segments from each subunit are α-helical and contribute to the lumen of the ion channel, possibly with additional contributions from the M1 segments, while amino acids from the M3 and M4 segments contribute to the lipid−protein interface (*4*, *5*).

In the GABA$_A$ receptor, mutational analyses have identified three positions, in the M1, M2, and M3 segments, which modulate the enhancing actions of alcohol and volatile anesthetics (*6*, *7*) and are hypothesized to contribute to an anesthetic binding pocket. In muscle nAChRs, substitutions at position M2-10′ modulate the inhibitory potency of long chain alcohols and isoflurane (*8*−*10*), while for neuronal nAChRs, substitutions at position M2-15′, a position identified in GABA$_A$ receptors as a potential contributor to an anesthetic binding site, as well as substitutions of the amino acids linking the M2 and M3 segments have been identified as determinants of volatile anesthetic sensitivity (*11*, *12*).

† This research was supported by grants from the National Institutes of Health [GM58448 (J.B.C.) and GM51595 (R.G.E.)] and by an award to Harvard Medical School in Structural Neurobiology from the Keck Foundation.

* To whom correspondence should be addressed. R.G.E.: Department of Anesthesia, University of Pennsylvania Medical Center, 311 John Morgan Bldg., 3620 Hamilton Walk, Philadelphia, PA 19104-6112; phone, (215) 662-3766; e-mail, Roderic.Eckenhoff@uphs.upenn.edu. J.B.C.: Department of Neurobiology, Harvard Medical School, 220 Longwood Ave., Boston, MA 02115; phone, (617) 432-1728; fax, (617) 734-7557; e-mail, jonathan_cohen@hms.harvard.edu.

‡ Harvard Medical School.

§ Current address: Department of Chemistry, Texas A&M University, College Station, TX 77843.

|| University of Pennsylvania.

[1] Abbreviations: Carb, carbamylcholine; dTC, *d*-tubocurarine; DTT, dithiothreitol; EDTA, ethylenediaminetetraacetate; EndoLys-C, endoproteinase Lys-C; GABA$_A$, γ-aminobutyric acid type A; HPLC, high-pressure liquid chromatography; nAChR, nicotinic acetylcholine receptor; OPA, *o*-phthalaldehyde; PAGE, polyacrylamide gel electrophoresis; SDS, sodium dodecyl sulfate; Tricine, *N*-tris(hydroxymethyl)-methylglycine; Tris, tris(hydroxymethyl)aminomethane; V8 protease, *Staphylococcus aureus* endopeptidase Glu-C.

10.1021/bi0351561 CCC: $25.00
Published on Web 10/29/2003

In the absence of atomic-resolution structures of these receptors in the presence of anesthetics, it is difficult to decide whether the positions where substitutions alter anesthetic potency contribute directly to anesthetic binding sites or are involved in the transduction mechanism and allosterically modulate anesthetic potency. Photoaffinity labeling provides a complementary approach to identifying amino acids contributing directly to drug binding sites (reviewed in refs *13* and *14*). For the nAChR, photoreactive agonists and antagonists have provided extensive identification of the amino acids contributing to the agonist binding sites and to the ion channel (*15*, *16*), and [^{3}H]azioctanol, a general anesthetic containing a photoreactive diazirine, reacted with high efficiency with αGlu-262 (M2-20′) at the C-terminal (extracellular) end of the M2 ion channel domain (*17*).

Halothane (2-chloro-2-bromo-1,1,1-trifluoroethane), a clinically important volatile anesthetic, produces anesthesia with an EC_{50} of 0.3 mM and inhibits nAChRs with IC_{50} values varying from 0.1 mM for some neuronal nAChR subtypes to 0.8 mM for muscle nAChRs (*18*). The carbon−bromine bond of halothane is unstable under UV irradiation, and the resultant radical intermediate reacts with fatty acids (*19*) and with poly(L-lysine) (*20*). In addition, [^{14}C]halothane can be photoincorporated into amino acids within soluble and integral membrane proteins (*21*), and individual photolabeled aromatic amino acids (tryptophans) have been identified within one of the fatty acid/drug binding sites of serum albumin (*22*), apomyoglobin (*23*; also His), and within the retinal binding pocket of rhodopsin (*24*). For *Torpedo* nAChR-rich membranes equilibrated with [^{14}C]halothane at anesthetic doses, brief UV irradiation resulted in covalent incorporation of ^{14}C into each nAChR subunit, with the level of photolabeling reduced by higher concentrations of nonradioactive halothane or isoflurane, but not by a nAChR agonist (carbamylcholine) or a competitive antagonist (α-bungarotoxin) (*25*). In this report, we use protein chemistry techniques to identify some of the nAChR amino acids photolabeled with [^{14}C]halothane.

EXPERIMENTAL PROCEDURES

Materials. nAChR-rich membranes were isolated from fresh *Torpedo californica* electric organs as described previously (*26*). Membranes contained 1−1.4 nmol of [^{3}H]-ACh binding sites per milligram of protein and were stored until they were used at a concentration of 4−8 mg of protein/mL at −80 °C in 38% sucrose and 0.02% sodium azide. [^{14}C]Halothane (50 mCi/mmol) was obtained as a custom synthesis from New England Nuclear and was used shortly after being received to reduce the level of contamination from β-degradation products. The material was routinely verified to have >95% of the radioactivity in the halothane HPLC peak prior to being used. Nonradioactive halothane and isoflurane were from Halocarbon Laboratories (Hackensack, NJ) and Anaquest, Inc. (Madison, WI). Carbamylcholine and *d*-tubocurarine were from Sigma. 1-Azidopyrene was from Molecular Probes. *Staphylococcus aureus* glutamyl endopeptidase (V8 protease) was purchased from ICN Biomedical, endoproteinase Lys-C (EndoLys-C) from Roche Biochemical, and TPCK-treated trypsin from Worthington Biochemical.

Photolabeling nAChR-Rich Membranes with [^{14}C]Halothane. nAChR-rich membranes were resuspended at a concentration of 1.5 mg of protein/mL in deoxygenated *Torpedo* physiological saline [250 mM NaCl, 5 mM KCl, 3 mM $CaCl_2$, 2 mM $MgCl_2$, and 5 mM sodium phosphate (pH 7.0)] and equilibrated under argon for 30 min on ice prior to photolabeling. Reagents were assembled in Teflon-stoppered quartz 2 mL cuvettes to achieve the concentrations listed in Results, with [^{14}C]halothane being the final addition. Samples were mixed and equilibrated for 1 min before being irradiated for 60 s with an Oriel low-pressure Hg(Ar) pencil calibration lamp at 5 mm with constant mixing. The dominant peak from this source is at 254 nm. The cuvette contents were diluted 10-fold and washed iteratively by centrifugation.

To visualize nAChR subunits resolved by preparative SDS−PAGE without staining and destaining the gel, after photolysis with [^{14}C]halothane, membrane suspensions were photolabeled with 1-azidopyrene, a fluorescent photoreactive hydrophobic compound (*27*), and then pelleted and washed as described above.

Gel Electrophoresis. Photolabeled nAChR-rich membranes were separated by SDS−PAGE as described previously (*28*). After electrophoresis, the unstained gel was visualized under UV light, and the nAChR subunits were excised on the basis of the fluorescence of the incorporated 1-azidopyrene. The subunit bands were eluted, filtered, concentrated, acetone precipitated, and resuspended as described previously (*29*). For fluorography, gels were treated with Amplify (Amersham Pharmacia Biotech), dried, and exposed to Kodak X-OMAT AR film at −80 °C. For quantitation of the ^{14}C in gel slices, slices were soaked in 5 mL of gel cocktail [90% toluene, 10% TS-2 tissue solubilizer (Research Products International Corp.) with 12.6 mM 2,5-diphenyloxazole and 770 μM 1,4-bis(5-phenyloxazol-2-yl)benzene] for 3−5 days and counted.

Enzymatic Digestions. In-gel digestions of the nAChR α subunit with *S. aureus* V8 protease were carried out as described previously (*30*). Solution digestions with V8 protease (1:1, w:w, 25 °C, 2−3 days) were performed in storage buffer [10 mM $NaPO_4$, 1 mM DTT, 1 mM EDTA, and 0.1% SDS (pH 7.0)]. For digestion with EndoLys-C (0.5−1 unit/digest, 3 weeks, 25 °C), the subunits and/or fragments were resuspended in 25 mM Tris, 0.5 mM EDTA, and 0.1% SDS (pH 8.6). Trypsin digests (1:1, w:w, 2−3 days, 25 °C) were performed in storage buffer supplemented with 0.5% Genapol C-100 (Calbiochem).

Reversed-Phase HPLC. HPLC separations and/or purifications of nAChR subunit fragments were performed using either Waters 510 pumps controlled by a 680 gradient controller or an Agilent 1100 Binary HPLC system with a degasser and column heating compartment (set at 40 °C). Separations were achieved using a Brownlee Aquapore butyl 7 μm, 100 mm × 2.1 mm column with a C-2 guard column. HPLC solvents are noted in the figure legends, and gradients are included in the figures.

N-Terminal Sequence Analysis. Edman degradation was performed on an Applied Biosystems 477 gas-phase sequencer modified to analyze one-third of each cycle with a 120A amino acid analyzer and to collect two-thirds of each cycle for scintillation counting. Data shown in the figures are the actual counts per minute (cpm) and background-subtracted picomoles (determined by peak height) of the

detected amino acid in each cycle. The picomoles detected were fit (nonlinear, least squares, SigmaPlot, SPSS Inc.) to the equation $f(x) = I_0R^x$, where $f(x)$ is the background-subtracted picomoles in cycle x, I_0 is the initial amount of peptide sequenced, and R is the repetitive yield. The fit of this equation is included as a dotted line in figures of sequence runs. Cys, Ser, Trp, and His were excluded from this analysis because of known problems with their quantitation via Edman degradation. The specific ^{14}C incorporation (cpm per picomole) in cycle x was calculated as $(\text{cpm}_x - \text{cpm}_{x-1})/(2I_0R^x)$. The total amount of peptide sequenced was assumed to be $3I_0$. HPLC fractions of interest were either drop-loaded onto Beckman peptide supports (no. 290111) placed on a 45 °C heating block or pooled, concentrated by centrifugal evaporation, resuspended in a minimal volume of 0.1% SDS (~40 μL), and loaded. When samples containing SDS were sequenced, the filters were first treated with gas trifluoroacetic acid (5 min) followed by an ethyl acetate wash (4 min) to remove excess detergent. In some cases, the sequencing run was interrupted and the material on the filter was treated with *o*-phthalaldehyde (OPA) as described previously (*26*). OPA reacts with primary amines preferentially over secondary amines (i.e., proline) and can be used at any sequencing cycle to block Edman degradation of peptides not containing an N-terminal proline (*31*).

Models of the Torpedo nAChR. A homology model of the *Torpedo* nAChR extracellular domain (N-terminus to the beginning of M1 for each subunit) was constructed from the structure of the AChBP (*32*) by using the Homology module in Insight II (Accelrys) on a Silicon Graphics O_2 workstation as described previously (*15*, *33*). The coordinates for the AChBP structure (Protein Data Bank entry 1I9B) and for the recently published structure (*34*) at 4 Å resolution of the *Torpedo* nAChR transmembrane domain (Protein Data Bank entry 1OED) were obtained from the Research Collaboratory for Structural Bioinformatics. The percent solvent exposures of the amino acids in the models that were labeled in the nAChR with [^{14}C]halothane were calculated by use of the access_surf function in the NMR module which determines the Connolly surface area of each amino acid in a structure using a 1.4 Å diameter ball.

RESULTS

Previous photolabeling of nAChR-rich membranes with [^{14}C]halothane demonstrated incorporation of ^{14}C into protein and lipid fractions. All nAChR subunits were labeled, and nAChR subunit labeling was not altered by the presence of agonist [carbamylcholine (Carb)] or antagonist (α-bungarotoxin), but the level of nAChR subunit labeling was reduced 75% by excess nonradioactive halothane, as was the extent of lipid labeling (*25*). To identify nAChR subunit amino acids photolabeled with [^{14}C]halothane, we carried out labelings on a preparative scale (~15 mg of protein, 7.5 nmol of nAChR) so that Edman degradation could be used to identify sites of ^{14}C incorporation in nAChR subunit fragments isolated by HPLC and/or SDS−PAGE. To also provide an initial definition of the pharmacological specificity of the photolabeling, membrane suspensions were photolabeled with [^{14}C]halothane in the absence of other drugs; in the presence of Carb, which would occupy the ACh sites and stabilize the nAChR in the desensitized state; in the presence of *d*-tubocurarine (dTC), a competitive antagonist; or in the presence of isoflurane, another volatile anesthetic.

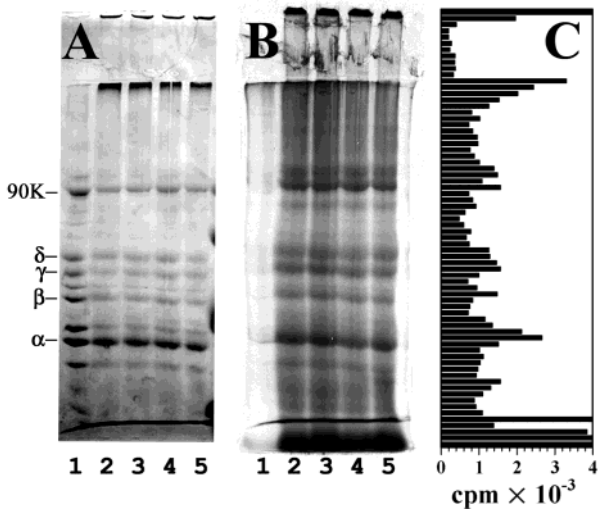

FIGURE 1: [^{14}C]Halothane photoincorporation into nAChR-rich membranes. nAChR-rich membranes (1 nmol of ACh sites/mg of protein, 2 mg/mL) were equilibrated (5 min) with 1 mM [^{14}C]-halothane alone (**3**) or with 7 mM isoflurane (**2**), 100 μM Carb (**5**), or 10 μM dTC (**4**). The suspensions were irradiated for 60 s at 254 nm. Aliquots (50 μg) were separated by SDS−PAGE (8% acrylamide) along with an unlabeled sample (**1**). Polypeptides were visualized with Coomassie blue (A), and the gel was processed for fluorography (B, 14 day exposure). (C) After fluorography, we cut lane 3 into 2 mm slices to quantitate the distribution of ^{14}C. The bottom of the sample well, the dye front, and the bottom of the gel contained 9400, 8200, and 9600 cpm, respectively. Indicated on the left are the Coomassie-stained bands corresponding to the nAChR subunits and the α subunit of the Na^+/K^+ ATPase (90K).

Figure 1 shows a Coomassie-stained 8% polyacrylamide gel and fluorogram with 50 μg aliquots from suspensions photolabeled with 1 mM [^{14}C]halothane under these four conditions. On the basis of the fluorogram, the presence of Carb, dTC, or isoflurane did not alter incorporation of ^{14}C into the nAChR subunits, and the ^{14}C distribution in the gel was similar to that of the Coomassie stain, with nAChR subunits and other polypeptides photolabeled as well as high-molecular mass aggregates produced by the UV irradiation. When ^{14}C incorporation for the control sample was quantified by liquid scintillation counting of 2 mm gel slice analysis (Figure 1C), there was a background distribution of ^{14}C throughout the gel at ~1000 cpm/gel slice, with ^{14}C incorporation in the nAChR α subunit at ~ 2000 cpm above background and in the β, γ, and δ subunits at ~1000 cpm. Since the 50 μg membrane aliquots contained ~50 pmol of nAChR α subunit and the specific activity of ^{14}C halothane was 50 Ci/mol, [^{14}C]halothane was incorporated into the nAChR α subunit at ~50 cpm/pmol or ~0.5 mol/mol of α subunit.

The level of incorporation of [^{14}C]halothane into the nAChR subunits was also estimated from the ^{14}C cpm and protein recovered from the preparative gel bands after the eluted material was precipitated with acetone and resuspended. From 15 mg of nAChR-rich membranes, we recovered 200−400 μg of the β, γ, and δ subunits with a ^{14}C incorporation of ~1000−1200 cpm/μg of protein, or ~0.5 mol of [^{14}C]halothane/mol of subunit. The incorporation of ^{14}C in those subunits was altered by less than 10% when nAChRs were labeled in the presence of Carb or isoflurane,

while labeling in the presence of dTC reduced the level of ^{14}C incorporation by 25−30%. Rather than elution of the gel bands containing the α subunit, they were transferred directly to a second "mapping" gel for digestion with *S. aureus* glutamyl endopeptidase (V8 protease).

To provide an initial map of the ^{14}C distribution within the nAChR α subunit, samples of the labeled α subunit were digested in gel with V8 protease to generate four large fragments of 20 (αV8-20), 18 (αV8-18), 10 (αV8-10), and 4 kDa (αV8-4) (*30*). αV8-20 begins at Ser-173 and contains ACh binding site segment C as well as the M1−M3 hydrophobic segments. αV8-18 begins at Val-46/Thr-52 and contains ACh binding site segments A and B. αV8-10 begins at Asn-339 and contains M4. αV8-4 begins at Ser-1. The bands corresponding to αV8-20, αV8-18, and αV8-10 were identified by Coomassie stain and excised, and the materials eluted from those bands were purified by reversed-phase HPLC and characterized by N-terminal sequence analysis. On the basis of the ^{14}C associated with the purified α subunit fragments and their picomole yields calculated by sequence analysis and/or protein determination, [^{14}C]halothane was incorporated in αV8-20 at a level of 30−50 cpm/pmol, in αV8-18 at 5−6 cpm/pmol, and in αV8-10 at 12−15 cpm/pmol. Labeling of nAChRs in the presence of Carb, dTC, or isoflurane did not alter the ^{14}C incorporation in αV8-10. Labeling in the presence of dTC reduced the level of ^{14}C incorporation in αV8-18 by ∼50%, while for Carb, the extent of labeling was not reduced. Difficulties in reliable quantification of the low mass levels that were sequenced precluded a similar analysis for the αV8-20 samples.

To determine whether the incorporated ^{14}C was generally stable to the necessary cycles of acid and base, which it was, and whether any amino acids near the amino terminus of the δ subunit were photolabeled, an aliquot of intact δ subunit isolated from nAChR-rich membranes photolabeled with [^{14}C]halothane in the presence of Carb was sequenced for 20 cycles (21 000 cpm loaded, 17 430 cpm left). There was no release of ^{14}C above background (<0.2 cpm/pmol).

We also collected the ^{14}C released during Edman degradation of HPLC-purified αV8-20, αV8-18, and αV8-10 to determine whether amino acids near their amino termini were photolabeled. When an aliquot of αV8-20 (4000 cpm) was sequenced, there was a 5 cpm release in cycles 9 and 12 above a background of 30 cpm, consistent with labeling of αTyr-181 and αTrp-184 at a low level (∼1 cpm/pmol), while the lack of release in earlier cycles indicated that any labeling of αTrp-176 (the other aromatic residue encountered) was at a level of <0.2 cpm/pmol. For αV8-10 (2400 cpm, beginning at αAsn-339), there was no release above background in 25 cycles, indicating that any labeling of αPhe-342 or αPhe-362 was at a level of <0.2 cpm/pmol. When an aliquot of αV8-18 (1200 cpm, beginning at αThr-52) was sequenced for 25 cycles, the only ^{14}C release above background was 6 cpm in cycle 21, consistent with labeling of αTyr-72 at ∼1 cpm/pmol, while the lack of release in earlier cycles established that any labeling of αTrp-60 or αTrp-67 was at a level of <0.2 cpm/pmol.

[^{14}C]Halothane Labeling in the δ Subunit: Photoincorporation in δM1 but Not δM2. To characterize [^{14}C]halothane photoincorporation in the δ subunit, we first digested the labeled subunit with endoproteinase Lys-C (EndoLys-C), a lysine-specific protease that produces δ subunit fragments

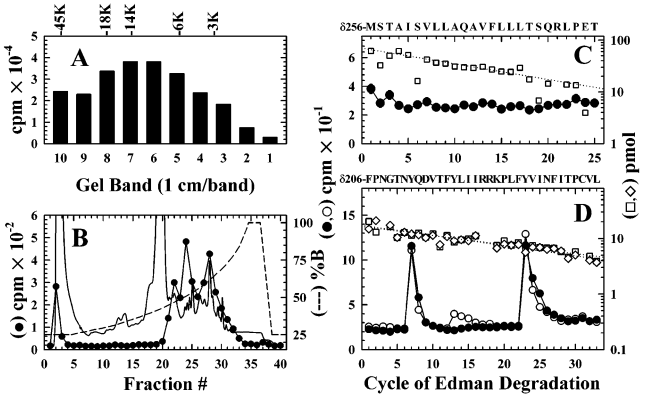

FIGURE 2: [^{14}C]Halothane photoincorporation in the nAChR δ subunit. The δ subunit (350 μg, 400 000 cpm) isolated from nAChR-rich membranes photolabeled with [^{14}C]halothane in the presence of 100 μM Carb was digested with EndoLys-C and separated on a Tricine gel (16.5% T/6% C). (A) The ^{14}C distribution eluted from 1 cm bands of the Tricine gel, with the mobilities of the prestained molecular mass markers indicated above. (B) Reversed-phase HPLC fractionation of material from band 6 (8−11 kDa). Solvent A was 0.05% trifluoroacetic acid in water; solvent B was 60% acetonitrile, 40% 2-propanol, and 0.08% trifluoroacetic acid. Plotted are the counts per minute per fraction [10% assayed (●)], the absorbance at 215 nm (—), and the HPLC gradient in % solvent B (- - -). (C) ^{14}C (●) and picomoles (□) detected during sequence analysis of HPLC fraction 28 (3700 cpm loaded, 2200 cpm remaining on the filter after 25 cycles). The primary sequence began at δMet-256, the beginning of δM2 (□, $I_0 = 70 \pm 3$ pmol, $R = 93 \pm 1\%$), and there was no ^{14}C release above background. (D) ^{14}C (● and ○) and picomoles (□ and ◇) detected during sequence analysis of two equal aliquots of the pool of HPLC fractions 24 and 25, with one sample (● and □) treated with *o*-phthalaldehyde (OPA) prior to cycle 2, corresponding to δPro-207 in the primary sequence. For both samples, the primary sequence began at δPhe-206 ($I_0 = 16 \pm 1$ pmol, $R = 96 \pm 1\%$); 3000 cpm was loaded, with 1300 (○) or 1800 cpm (●) remaining on the filter after 33 cycles. In the absence OPA, there was ^{14}C release in cycles 7 (87 cpm), 13 (16 cpm), and 23 (102 cpm), while after OPA treatment at cycle 2, there was ^{14}C release in cycles 7 (93 cpm) and 23 (91 cpm), but not in cycle 13. Thus, the ^{14}C release in cycle 13 did not originate from the δPhe-206 peptide.

of ∼21 kDa, beginning at δHis-20/δHis-26 and containing agonist site segments D and E (*35*); 10 kDa, beginning at δMet-257, the beginning of δM2 (*36*); and ∼12 kDa, beginning at δPhe-206 and containing a site of N-linked glycosylation (δAsn-208) and δM1 (*37*). When an EndoLys-C digest of the nAChR δ subunit from membranes photolabeled with [^{14}C]halothane (+Carb) was fractionated by Tricine SDS−PAGE (Figure 2A), the ^{14}C was distributed broadly throughout the gel, with no evidence of selective photolabeling in either the 10−13 kDa region or the 21 kDa region (similar distributions of ^{14}C were seen for EndoLys-C digests of δ subunits from membranes labeled with [^{14}C]-halothane in the absence of other ligands, or in the presence of isoflurane or dTC).

When the 10 kDa region of the Tricine gel (band 6) was concentrated and fractionated by reversed-phase HPLC, there was a broad distribution of ^{14}C eluting between fractions 21 and 30 (45−70% organic; Figure 2B). Similar ^{14}C elution profiles were seen for the HPLC purification of the 10 kDa bands from the four labeling conditions. When the most hydrophobic ^{14}C peak (fraction 28 at 62% organic) was sequenced (Figure 2C), the sample contained a single peptide beginning at δMet-257, the N-terminus of δM2 ($I_0 = 70$

pmol), and there was no ^{14}C release above background during the 25 cycles of degradation. In addition, no ^{14}C release was detected in sequence analysis of the equivalent δM2 fragments isolated from digests of the δ subunit from nAChRs labeled in the absence of other drugs or in the presence of dTC or isoflurane (not shown). The sample labeled with [^{14}C]-halothane in the absence of other drugs was sequenced for 40 cycles without any release of ^{14}C above background. Thus for δTyr-291 in δM3, which was present in cycle 35 (4.6 pmol), the maximum level of [^{14}C]halothane labeling was $<$0.3 cpm/pmol.

Sequence analysis (Figure 2D) of the peak of ^{14}C at 52% organic (fractions 24 and 25) from the HPLC fractionation in Figure 2B revealed a peptide beginning at δPhe-206, 19 amino acids before the start of δM1, with ^{14}C release (○) in cycles 7, 13, and 23, coinciding with δTyr-212, δTyr-218, and δTyr-228, respectively. To determine whether the sites of incorporation were indeed these tyrosines, we sequenced another aliquot of the pool, with the sequencing filter treated with *o*-phthalaldehyde (OPA) prior to cycle 2 [Figure 2D (●)] to prevent Edman degradation of fragments not containing a proline in the second cycle (*31*). This treatment demonstrated that only two of the tyrosine residues, δTyr-212 and δTyr-228, were photolabeled with [^{14}C]halothane. The ^{14}C release in cycle 13 from the sample not treated with OPA probably reflected labeling of δTyr-212 from a fragment produced by EndoLys-C cleavage after δLys-199 rather than δLys-205.

The equivalent HPLC fractions from the other three labeling conditions were sequenced with OPA treatment in cycle 2 (Figure 3). Under all conditions, [^{14}C]halothane photolabeled δTyr-212 and δTyr-228, but the efficiency of incorporation (counts per minute per picomole) at the two amino acids depended upon the labeling conditions. For δTyr-212, ^{14}C photoincorporation was unaffected by the addition of either isoflurane or Carb, but dTC reduced the level of incorporation by $>$90% (Figure 3E). For δTyr-228, [^{14}C]halothane incorporation was inhibited ~40% by isoflurane, whereas the extent of incorporation was *increased* in the presence of Carb and dTC, by 90 and 50%, respectively (Figure 3F).

Sequence analysis of the early ^{14}C peak from the HPLC fractionation in Figure 3B (fraction 22) revealed a peptide from the β subunit of the sodium potassium ATPase, a known contaminant of the nAChR δ subunits isolated by SDS−PAGE from nAChR-rich membranes (*29*).

Photoincorporation of [^{14}C]Halothane in α*M4,* α*M1, and* α*V8-18.* Since sequence analysis of the N-termini of the α subunit proteolytic fragments provided evidence of low-level labeling of some tyrosines, we digested and fractionated αV8-20 to determine whether [^{14}C]halothane reacted with any of the aromatics within the nAChR αM1 hydrophobic segment (αTyr-213/αPhe-214), and we digested and fractionated αV8-10 to determine whether amino acids were labeled within αM4, which contains no aromatics, or whether αTyr-401, which precedes αM4 in the primary structure, was labeled. In addition, we wanted to determine whether the labeling within αV8-18 was associated with αTyr-93, one of the aromatic amino acids in the ACh binding site.

A fragment beginning at αTyr-401 can be readily isolated by reversed-phase HPLC purification of trypsin digests of

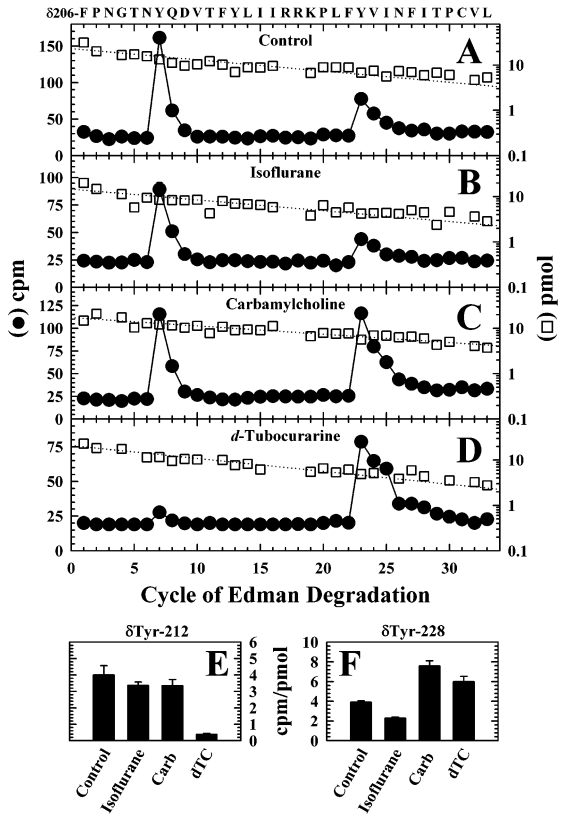

FIGURE 3: Pharmacological effects on [^{14}C]halothane photoincorporation at δTyr-212 and δTyr-228. Aliquots of the δ subunit isolated from nAChR-rich membranes photolabeled in the presence of [^{14}C]halothane alone (A) or with isoflurane (B), Carb (C), or dTC (D) were digested with EndoLys-C and separated by Tricine SDS−PAGE, and material that eluted from the ~10 kDa region was fractionated by HPLC. Aliquots of a pool of the fractions known to contain the peptide beginning at δPhe-206 (fractions 24 and 25) were sequenced for each labeling condition, with OPA treatment in the second cycle to prevent sequencing of contaminating peptides. For each sample, after OPA treatment, the only detectable sequence began at δPhe-206 [□, (A) $I_0 = 23 \pm 2$ pmol, $R = 95 \pm 1\%$; (B) $I_0 = 15 \pm 1$ pmol, $R = 95 \pm 1\%$; (C) $I_0 = 17 \pm 1$ pmol, $R = 96 \pm 1\%$; (D) $I_0 = 21 \pm 1$ pmol, $R = 94 \pm 1\%$]. In all samples, release of ^{14}C (●) was detected in cycle 7 [(A) 137 cpm, (B) 66 cpm, (C) 93 cpm, and (D) 12 cpm] and cycle 23 [(A) 50 cpm, (B) 21 cpm, (C) 91 cpm, and (D) 60 cpm] corresponding to δTyr-212 and δTyr-228, respectively. In addition to these two labeled tyrosine residues, an unlabeled tyrosine residue was also encountered within the 33 cycles of Edman degradation, δTyr-218. Three to four sequence runs were performed for each condition, and the calculated averages (and standard deviation) of counts per minute of [^{14}C]halothane per picomole of δTyr-212 and δTyr-228 are shown in panels E and F, respectively.

αV8-10 (*27*). When a trypsin digest of gel-purified αV8-10 was fractionated by reversed-phase HPLC, the fragment beginning at αTyr-401 was recovered as a hydrophobic peak of ^{14}C centered at fraction 35 (Figure 4A). Sequence analysis (Figure 4C) established that the primary sequence began at αTyr-401 ($I_0 = 72$ pmol), with a secondary sequence beginning at αSer-388 ($I_0 = 15$ pmol). The only ^{14}C release above background was in cycle 12 (40 cpm), which corresponded to either labeling of αCys-412 in the primary sequence at ~0.9 cpm/pmol or labeling of αTrp-399 in the secondary sequence at 9 cpm/pmol. (In two other [^{14}C]-halothane labeling experiments, αV8-10 was similarly processed to isolate these same two peptides, and the calculated levels of ^{14}C incorporation in the cycle 12 residues

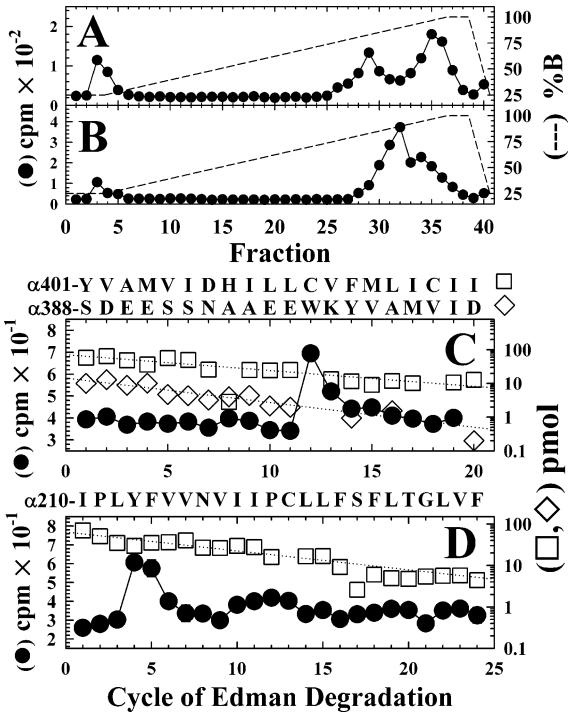

FIGURE 4: [^{14}C]Halothane photoincorporation in αV8-10 and αV8-20. Aliquots of [^{14}C]halothane-labeled αV8-10 [(A) 21 000 cpm] and αV8-20 [(B) 63 000 cpm] were digested with trypsin and separated by reversed-phase HPLC with the same solvents as in Figure 2. Five percent of each fraction was assayed for ^{14}C (●), and the gradients are shown (- - -). For the αV8-10 digestion, fractions 34−36 (95% organic) were pooled and sequenced [(C) ●, 3670 cpm loaded, 2650 cpm left after 20 cycles]. The primary and secondary sequences began at αTyr-401 (□, $I_0 = 72 \pm 6$ pmol, $R = 90 \pm 1\%$) and αSer-388 (◇, $I_0 = 15 \pm 2$ pmol, $R = 85 \pm 2\%$). The ^{14}C release (35 cpm) in cycle 12 would correspond to labeling of αCys-412 (0.9 cpm/pmol) or αTrp-399 (9 cpm/pmol) in the primary or secondary sequence. For the αV8-20 digestion, fractions 34−37 (95% organic) were pooled and sequenced [(D) ●, 5100 cpm loaded, 3250 cpm left after 24 cycles] with the sequencing filter treated with OPA after the first cycle to prevent sequencing of peptides without a proline in cycle 2. After OPA, the only fragment detected began at αIle-210 (□, $I_0 = 64 \pm 5$ pmol, $R = 90 \pm 1\%$), and the ^{14}C release (30 cpm) in cycle 4 corresponded to labeling of αTyr-213 (0.4 cpm/pmol) in αM1.

were 11 and 11 cpm/pmol for αCys-412 and 2.3 and 2.7 cpm/pmol for αTrp-399.)

To characterize ^{14}C incorporation in αM1, we took advantage of the fact that there is a trypsin cleavage site (αArg-209) followed by a proline (α211). In a trypsin digest of αV8-20, labeling within αM1 can be characterized by use of OPA in the second cycle of Edman degradation (*38*). When a trypsin digest of gel-purified αV8-20 was fractionated by reversed-phase HPLC, the ^{14}C was recovered in a broad hydrophobic peak (Figure 4B). Fractions 34−37 were pooled and sequenced, and the sample filter was treated with OPA at cycle 2 (Figure 4D). After the second cycle, the only sequence that was detected was αM1 Ile-210 ($I_0 = 64$ pmol). There was ^{14}C release in cycle 4 (30 cpm), consistent with labeling of αTyr-213 at a level of ∼0.4 cpm/pmol.

Trypsin digestion of αV8-18 produces a fragment readily purified by reversed-phase HPLC that begins at αLeu-80 and contains αTyr-93 (as well as αPro-81) (*39*). When we fractionated a trypsin digest of [^{14}C]halothane-labeled αV8-18 by reversed-phase HPLC (Figure 5A), there was a peak of ^{14}C in fractions 20 and 21 (∼40% organic) at the position

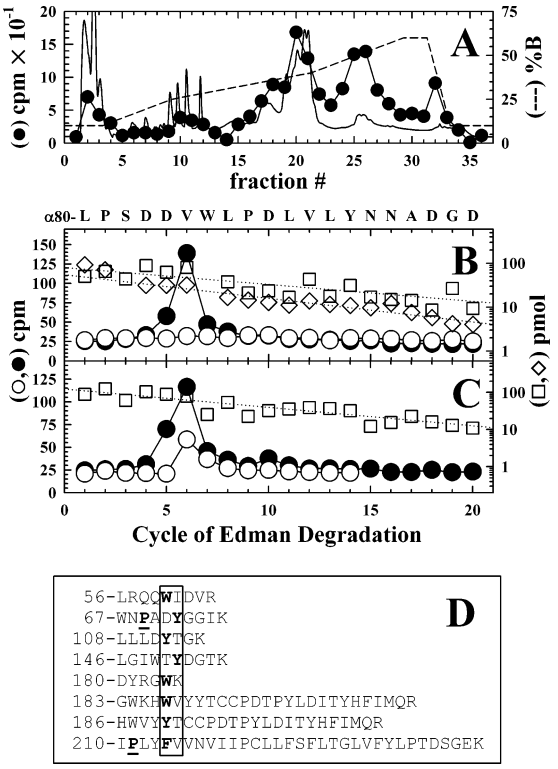

FIGURE 5: [^{14}C]Halothane photoincorporation in αV8-18. Agonist site residue αTyr-93 is not labeled. Aliquots of αV8-18 isolated from V8 mapping gels of the α subunit labeled with [^{14}C]halothane as described in the legend of Figure 1 were digested with trypsin and separated by reversed-phase HPLC as described previously (*39*) to isolate a fragment beginning at αLeu-80 that contains αTyr-93 of ACh binding site segment A. (A) HPLC elution profile with 10% of each fraction assayed for ^{14}C (●), the absorbance at 215 nm (—), and the HPLC gradient in % solvent B (- - -). (B) HPLC fractions 20 and 21 were pooled, and two aliquots were sequenced, without (● and □, 1100 cpm loaded, 370 cpm left after 20 cycles) or with (○ and ◇, 1100 cpm loaded, 670 cpm left after 20 cycles) OPA treatment in cycle 2. The primary sequence in the untreated sample and the only sequence in the treated sample began at αLeu-80 (□, $I_0 = 79 \pm 10$ pmol, $R = 92 \pm 1\%$; ◇, $I_0 = 55 \pm 5$ pmol, $R = 88 \pm 1\%$). Since the ^{14}C release in cycles 5 (25 cpm) and 6 (81 cpm) in the untreated sample was eliminated upon OPA treatment at αPro-81, this [^{14}C]halothane incorporation was not associated with the fragment beginning at αLeu-80. (C) Fractions 20−22 from a similar HPLC separation of the +Carb sample were pooled, and two aliquots were sequenced, without (● and □, 1660 cpm loaded, 260 cpm left after 20 cycles) and with (○, 1660 cpm loaded, 400 cpm left after 20 cycles) OPA treatment in cycle 3. This sample contained the same primary sequence beginning at αLeu-80 (□, $I_0 = 123 \pm 13$ pmol, $R = 89 \pm 2\%$), which was eliminated upon OPA treatment at αSer-81. There was ^{14}C release in cycles 5 (39 cpm) and 6 (46 cpm) in the untreated sample, and after OPA treatment, the release in cycle 5 was eliminated while the release in cycle 6 remained (38 cpm). (D) Predicted tryptic peptides from αV8-18 and αV8-20 that contain an aromatic amino acid in cycle 5 or 6. The ^{14}C release in cycle 6 after treatment with OPA in cycle 3 would be consistent with [^{14}C]halothane labeling of αTyr-72 in a decapeptide beginning at αTrp-67.

expected for the αLeu-80 peptide. Sequence analysis (Figure 5B) revealed the peptide beginning at αLeu-80 ($I_0 = 79$ pmol), with ^{14}C release (●) in cycles 5 and 6 (25 and 100 cpm, respectively), but not in cycle 14 which corresponded to αTyr-93. The ^{14}C release in cycles 5 or 6 did not result from labeling of αAsp-84/αVal-85, since no ^{14}C release was observed when an aliquot was sequenced with OPA treatment in cycle 2 (○), a treatment that did not prevent the sequencing

of the αLeu-80 peptide. Therefore, the labeled amino acids contributing to this release must be in peptides present at mass levels that are too low for detection, which would be most likely for small peptides where the labeled and unlabeled peptides were separated by reversed-phase HPLC. Among the possible tryptic fragments from αV8-18 and αV8-20 (which is also present in gel-purified αV8-18), there are eight peptides with aromatic residues in cycle 5 or 6 (Figure 5D). One, in particular, a decapeptide beginning at αTrp-67, contains a proline in cycle 3 (αPro-69) and a tyrosine in cycle 6 (αTyr-72). To determine whether ^{14}C release in cycle 6 might result from labeling of αTyr-72, we sequenced another aliquot with OPA treatment in cycle 3 [Figure 5C (○)]. After this treatment, the ^{14}C release in cycle 6 was preserved, while the sequencing of the αLeu-80 fragment terminated in cycle 3. Therefore, [^{14}C]halothane is photoincorporated in αTyr-72, as had been suggested in the N-terminal sequence analysis of αV8-18.

[^{14}C]Halothane Labeling in Segment E of the Agonist Binding Site. As a first step at characterization of [^{14}C]-halothane photoincorporation within the nAChR γ subunit, we digested the labeled γ subunit with V8 protease and fractionated the digest by Tricine SDS−PAGE to isolate a 14 kDa fragment beginning at γVal-102 (*40*) which contains γTyr-111 and γTyr-117 of agonist binding site segment E. This 14 kDa band was further purified by reversed-phase HPLC (Figure 6A). Sequence analysis of HPLC fractions 25 and 26 (Figure 6B) revealed the peptide beginning at γVal-102 along with fragments of V8 protease. In 25 cycles of Edman degradation, there was ^{14}C release in cycles 4, 10, and 16 corresponding to γTyr-105 (1 cpm/pmol), γTyr-111 (5 cpm/pmol), and γTyr-117 (2 cpm/pmol), respectively, with no release above background in cycle 3 or 23 corresponding to γTyr-104 or γTyr-124, respectively. From a separate labeling, V8 protease digests of γ subunits isolated from nAChR-rich membranes photolabeled with [^{14}C]halothane in the presence of isoflurane, Carb, or dTC were fractionated by reversed-phase HPLC, and the fractions containing the γVal-102 peptide were pooled and sequenced. In the +isoflurane (Figure 6C) and +Carb (Figure 6D) samples, there was ^{14}C release in cycles 4 and 10 corresponding to γTyr-105 (3 and 2 cpm/pmol, respectively) and γTyr-111 (6 and 1 cpm/pmol, respectively), whereas for the +dTC (Figure 6E) sample, release was only detected in cycle 4 corresponding to γTyr-105 (0.8 cpm/pmol). For the +dTC sample, the level of labeling at γTyr-111 was <0.1 cpm/pmol. None of the samples had ^{14}C release in cycle 3 corresponding to γTyr-104.

DISCUSSION

In this report, we identify the nAChR structural domains and some of the amino acids that are photolabeled by the volatile anesthetic [^{14}C]halothane, and we have begun to characterize the pharmacological specificity of the photolabeling. Irradiation at 254 nm was used for photoactivation, which will produce halothane radical and may produce reactive intermediates of aromatic amino acids or cystine. We first describe the location of the labeled and unlabeled amino acids within the structure of the nAChR, and then we discuss the implications of the photolabeling results for the mechanism of inhibition of nAChRs by halothane.

[^{14}C]Halothane Labeling within the nAChR Extracellular and Transmembrane Domains. [^{14}C]Halothane was incorporated within each subunit at ∼50 cpm/pmol (or 0.5 mol of halothane/mol of subunit), with labeling distributed among a number of amino acids, primarily tyrosines, and no single labeled amino acid accounted for more than 10−15% of the subunit labeling. We summarize in Table 1 the labeling efficiencies of the aromatic amino acids that we identified as labeled (or unlabeled), as well as their location within the nAChR. In Table 1, we also include the calculated Connolly surface exposure of the side chains from their location in a homology model of the nAChR extracellular domain based upon the structure of the AChBP (*32*) (Figure 7) or in the recently published structure at 4 Å resolution of the *Torpedo* nAChR transmembrane domain (*34*). For the 14 Tyr and 5 Trp residues that were characterized, there was no significant correlation between labeling efficiency and predicted aqueous exposure ($r = 0.19$, $P = 0.44$), showing that labeling is not dominated by access as might be expected for nonspecific labeling. Amino acids identified as labeled (or unlabeled) in the nAChR extracellular domain are shown in Figure 7, and Figure 8 shows the location of the three Tyr residues characterized in the δ subunit transmembrane domain.

Within the extracellular domain, γTyr-111, in agonist binding site segment E, was one of the amino acids labeled at highest efficiency (5 cpm/pmol), while αTyr-93, which forms one of the sides of the quaternary ammonium binding pocket, was unlabeled (<0.1 cpm/pmol). Although we did not characterize the labeling within αTyr-190 or αTyr-198 in agonist site segment C, δTyr-212, which is the position in the δ subunit equivalent to αTyr-198, contributes to a pocket similar to the agonist site and was labeled (4 cpm/pmol). Additional labeled amino acids include γTyr-105 (2 cpm/pmol), which is predicted to be exposed in a cleft within the vestibule of the ion channel, and αTyr-72 (1 cpm/pmol), which is in a freely accessible position at the "top" of the nAChR. However, δTyr-218, which is also predicted to be exposed, was not labeled (<0.1 cpm/pmol). Although we have no direct proof that δTyr-218 is surface accessible, based upon lysine scanning mutagenesis, the equivalent position in the nAChR ϵ subunit is predicted to be surface-exposed (*41*). In addition to the identification of labeled amino acids, the fact that γTyr-105 is labeled at least 10-fold more efficiently than γTyr-104 provides dramatic evidence of strong steric constraints on the labeling of tyrosines, and the lack of labeling of γTyr-104 is consistent with its predicted orientation toward the subunit interior.

Few labeled amino acids were identified in the nAChR transmembrane domain. δTyr-228 within δM1 was one of the most highly labeled nAChR amino acids (4 cpm/pmol; see below for pharmacological specificity), and αTyr-213, next to the corresponding position in the α subunit, was also labeled. In the closed state structure of the nAChR δ subunit transmembrane domain, δTyr-228 projects into an extracellular, water-accessible pocket that is large enough to accommodate halothane (Figure 8) or isoflurane. This pocket is formed by amino acids from M1−M3, including the unlabeled δTyr-291 in δM3. δTyr-248, the only aromatic side chain characterized that is exposed at the lipid interface, was also unlabeled. No labeling was detected within δM2, but there are no aromatic amino acids within any of the M2

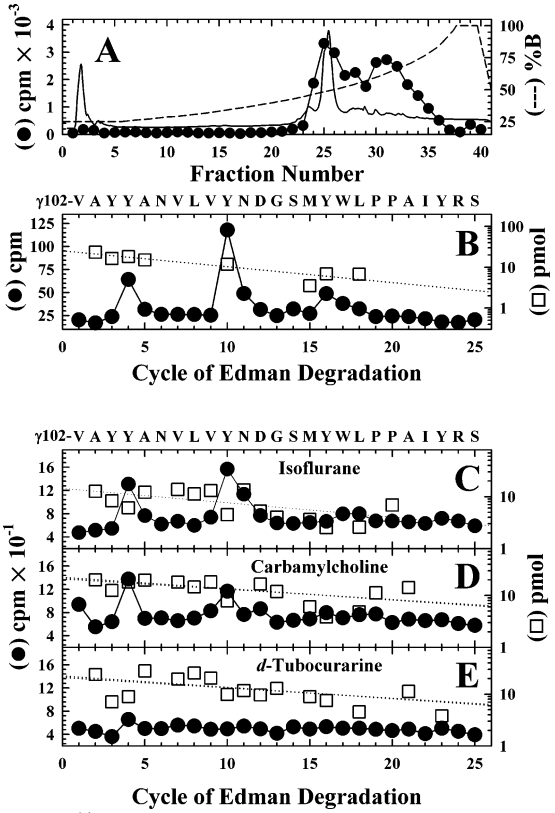

FIGURE 6: [^{14}C]Halothane incorporation in segment E of the α-γ agonist site. Differential inhibition by Carb and dTC. (A and B) Fifteen milligrams of nAChR-rich membranes (1.3 nmol of ACh binding sites/mg of protein) in 10 mL of TPS were equilibrated with 440 μM [^{14}C]halothane (52 mCi/mmol), photolyzed (254 nm, 100 s), and then labeled with 1-azidopyrene. Polypeptides were separated by SDS−PAGE, and the γ subunit was detected by fluorescence, excised, and eluted (420 000 cpm). The labeled γ subunit was digested with V8 protease (440 μg in 250 μL of 0.1 M NH_4HCO_3 with 0.1% SDS, 5 days, 25 °C), and the digest was fractionated by Tricine SDS−PAGE (16.5% T/6% C). (A) A band of ∼14 kDa was excised, eluted, and separated by reversed-phase HPLC. Solvents were as described in the legend of Figure 2, and the gradient (- - -) is shown in % solvent B. The solid line is the absorbance at 214 nm, and the dotted line is the fluorescence. Ten percent of each fraction was assayed for ^{14}C (●). (B) Sequence analysis of the ^{14}C peak at ∼48% solvent B (fractions 24−26, 4900 cpm loaded, 3150 cpm left after 25 cycles of Edman degradation). The primary γ subunit sequence began at γVal-102 (□, $I_0 = 25 \pm 2$ pmol, $R = 91 \pm 1\%$), and there was a fragment of V8 protease beginning at Val-1 (400 pmol). The ^{14}C release (●) in cycles 4 (40 cpm), 10 (93 cpm), and 16 (21 cpm) corresponded to labeling of γTyr-105, γTyr-111, and γTyr-117, respectively, from the γVal-102 peptide. (C−E) Samples of the γ subunit (120 000 cpm, 90 μg for +isoflurane, 120 000 cpm, 140 μg for +dTC, and 200 000 cpm, 180 μg for +Carb) from the labeling described in the legend of Figure 1 were digested with V8 protease (40 μg in 150 μL of storage buffer for 2 days at 25 °C) and separated by reversed-phase HPLC as described previously (*40*). Fractions 12−14 (∼25% organic) were pooled and sequenced for each condition [●, (C) with isoflurane, 8200 cpm loaded, 4800 cpm left after 25 cycles of Edman degradation; (D) with Carb, 15 500 cpm loaded, 8900 cpm left after 25 cycles of Edman degradation; (E) with dTC, 8700 cpm loaded, 6100 cpm left after 25 cycles]. For each sample, the primary γ subunit sequence began at γVal-102 [□, (C) with isoflurane, $I_0 = 14 \pm 3$ pmol, $R = 93 \pm 3\%$; with Carb, $I_0 = 21 \pm 3$ pmol, $R = 96 \pm 2\%$; with dTC, ◇, $I_0 = 23 \pm 4$ pmol, $R = 95 \pm 2\%$]. Also present in each was a fragment of V8 protease beginning at Val-1 (with isoflurane, 85 pmol; with Carb, 177 pmol; and with dTC, 117 pmol). In the +isoflurane and +Carb samples, the ^{14}C release in cycles 4 and 10 corresponded to labeling of γTyr-105 (84 and 73 cpm) and γTyr-111 (84 and 34 cpm), respectively. The only ^{14}C release in the +dTC sample occurred in cycle 4 (30 cpm).

Table 1: [^{14}C]Halothane Photoincorporation in nAChR Tyrosines and Tryptophans

amino acid	^{14}C incorporation (cpm/pmol)	predicted location[a]	% exposure[b]	lysine scan tolerance[c]
δTyr-17 (+Carb)	ND (<0.2)	helix 1	0	
αTrp-60	ND (<0.2)	β strand 2	1	N
αTrp-67	ND (<0.2)	loop 3 (β2−β3)	12	
αTyr-72	1	loop 3 (β2−β3)	85	
αTrp-86	ND (<0.1)	loop 4 (β3−β4)	2	
αTyr-93	ND (<0.1)	β strand 4	14	T
γTyr-104	ND (<0.1)	β strand 5−β strand 5′	1	T
γTyr-105	1.1	β strand 5−β strand 5′	17	T
γTyr-111	4.5	β strand 5′	32	T
γTyr-117	1.8	β strand 6	29	T
αTrp-176	ND (<0.2)	β strand 9	5	N
αTyr-181	1	β strand 9	5	N
αTrp-184	1	β strand 9	51	T
δTyr-212	4.0	β strand 10	10	T
δTyr-218	ND (<0.1)	β strand 10	25	T
δTyr-228	3.9	M1	66	
αTyr-213	0.4	M1	90	
δTyr-248 (+dTC)	ND (<0.2)	M1	*d*	
δTyr-291	ND (<0.3)	M3	55	
γTyr-286 (+Iso)	ND (<0.2)	M3	40	
αTyr-401	ND (<0.1)	Pre M4		

[a] For the extracellular domain, location in the secondary structure assignment of AChBP (*32*). [b] Connolly aqueous surface exposure in the *Torpedo* nAChR homology model or the structure of the *Torpedo* nAChR transmembrane domain (*34*), as calculated using the NMR-Refine module in Insight II. [c] Tolerance for Lys substitution in the nAChR ϵ subunit [T, tolerated; N, not tolerated (*41*)]. [d] The published structure predicts 30% lipid exposure for this Tyr. ND, not detected. For determination of the correlation between labeling efficiency and calculated aqueous surface exposure, labeling at the detection limit was assumed for the amino acids identified as ND. Where indicated, the sequenced fragment came from membranes photolabeled with [^{14}C]halothane in the presence of Carb (+Carb), dTC (+dTC), or isoflurane (+Iso).

segments. Although there was no evidence of labeling in γM3, δM3, or δM2 at amino acids equivalent to the positions in the $GABA_A$ receptor α subunit identified as volatile anesthetic affinity determinants (*6*, *7*), those positions are within a narrow extension of the aqueous pocket containing δTyr-228 which would not contain halothane in the nAChR closed state structure. Within αM4, αCys-412 which is exposed to lipid might be labeled, but we were unable to make a positive identification because all samples that we sequenced to characterize labeling within M4 contained two fragments, beginning at αTyr-401 and αSer-388, with αCys-412 and αTrp-399 in the 12th sequencing cycle where there was ^{14}C release.

Are Amino Acids Other than Tyr Labeled? αTrp-184 in the extracellular domain was labeled at a level of 1 cpm/pmol, as was αTrp-399 (cytoplasmic domain) and/or αCys-412 (in αM4). We were surprised that tryptophans were not labeled more prominently, since that was the amino acid labeled most efficiently within serum albumin and rhodopsin (*22*, *24*), where it was labeled within a fatty acid binding pocket and the chromophore binding pocket in the transmembrane domain, respectively. However, there are only nine Trp residues in the nAChR α subunit, with seven in the extracellular domain and two in the cytoplasmic domain. We did not determine the labeling of αTrp-118 or αTrp-

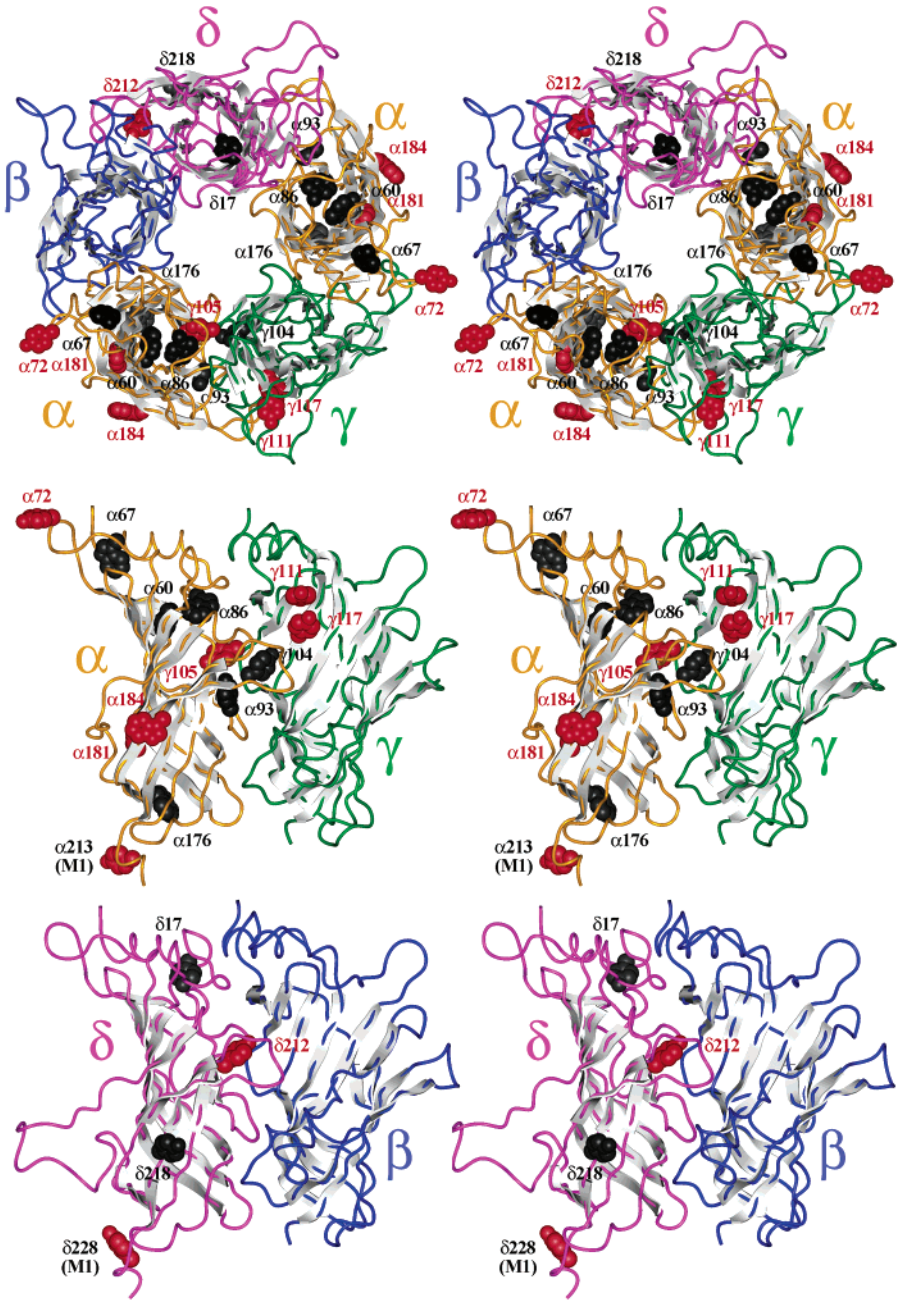

FIGURE 7: Spatial distribution of aromatic residues labeled with [^{14}C]halothane. Stereoviews of ribbon diagrams of the *Torpedo* nAChR extracellular domain modeled after the AChBP, with tyrosine and tryptophan side chains represented in CPK that were shown to be labeled with [^{14}C]halothane (red) or unlabeled (black). The top panel shows the pentameric subunit arrangement as viewed from the synaptic cleft. The middle and bottom panels are side views of the α and γ subunits and the δ and β subunits, respectively. Also included in all figures is the β-sheet secondary structure (gray). As the crystal structure of the AChBP ends at the amino acid homologous to the conserved proline residue at the beginning of M1 in the nAChR, we added five amino acids in a helical conformation to the side views of the α and δ subunits to illustrate the likely proximity of αTyr-213 and δTyr-228.

149, but we did sequence through the other five Trp residues in the extracellular domain and established that only αTrp-184 was labeled. On the basis of the structure of the AChBP, the four unlabeled Trp residues are all within the subunit interior with no surface accessibility, with αTrp-60 and αTrp-86 being two of nine amino acids absolutely conserved between the AChBP and this superfamily.

The limited number of identified amino acids labeled in the transmembrane domain was surprising. When the ^{14}C distribution was characterized within the large α subunit fragments that can be produced by V8 protease, we found most within αV8-20 (30−50 cpm/mol), with a lower level of labeling in αV8-10 (12−15 cpm/pmol), which contains αM4, and in αV8-18 (5−6 cpm/pmol), which contains agonist site binding segments A and B and most of the primary structure of the extracellular domain. It is possible that there is ^{14}C incorporation in the nAChR transmembrane domain that is refractory to Edman degradation, as would happen if the trifluorochloroethyl radical reacted with the amide backbone. Alternately, reaction with the unsaturated fatty acids within the phospholipid could result in ^{14}C-labeled fatty acid radical intermediates that might react with the nAChR, yielding modified amino acids that cannot be detected by Edman degradation.

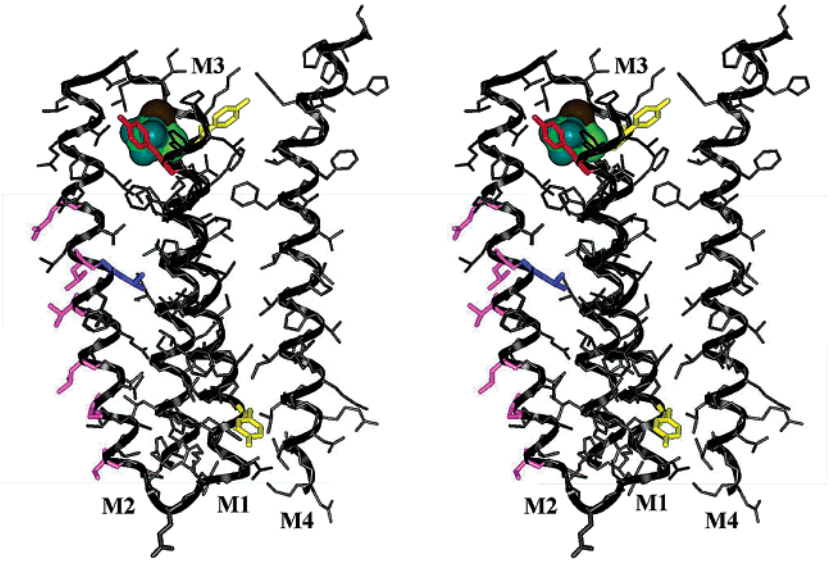

FIGURE 8: nAChR δ subunit transmembrane domain that contains a pocket formed by the M1−M3 helix bundle that can accommodate halothane near δTyr-228. A stick and ribbon stereomodel of the δ subunit transmembrane domain from the nAChR in the closed state is shown (*34*), oriented with the extracellular surface up and the approximate level of the lipid bilayer as a gray background. Also included is a Connolly surface representation of halothane manually placed within the existing pocket formed by the M1−M3 helices. Shown in red is δTyr-228 in M1 that is labeled with halothane and in yellow the unlabeled δTyr-291 in M3 as well as the unlabeled δTyr-248 in M1 that is exposed at the lipid interface. M2 residues identified as lining the lumen of the ion channel are in magenta. Shown in blue is M2-15′, a position in the $GABA_A$ receptor identified as an anesthetic sensitivity determinant.

State-Dependent Photolabeling by [^{14}C]Halothane within δM1. Analysis of the ^{14}C incorporation within a fragment beginning at δPhe-206 provided evidence that halothane and isoflurane bind within a site containing δTyr-228 in a pocket at the extracellular end of the nAChR transmembrane domain and that occupancy or accessibility is increased in the desensitized state compared to the closed channel state. Carb and dTC increased the level of labeling of δTyr-228 by 90 and 50%, respectively, while isoflurane reduced the level of labeling by 40%. Since for *Torpedo* nAChRs Carb fully stabilizes the desensitized state and dTC desensitizes it by 60% (*42*), this indicates increased accessibility of δTyr-228 to halothane in the desensitized state. Since isoflurane also desensitizes nAChRs (*43*), the reduced level of labeling in the presence of isoflurane is evidence of competition with halothane. The halothane labeling of δTyr-228 and αTyr-213 establishes that halothane interacts with a nAChR domain previously implicated in the gating mechanism. Cys substitutions at the equivalent position in the α and β subunits perturb gating, and the accessibility of αTyr-213Cys for chemical modification is increased by agonist (*44*−*46*).

Pharmacological Specificity of [^{14}C]Halothane Labeling in the nAChR Extracellular Domain. We compared the effects of Carb, dTC, and isoflurane on [^{14}C]halothane photolabeling of δTyr-212, which is not part of the ACh site but is an exposed amino acid in the δ subunit that is equivalent to αTyr-198 of the agonist binding site. This position in a $GABA_A$ receptor α subunit contributes to the benzodiazepine binding site (*47*) and is photolabeled with [^{3}H]Ro15-4513 (*48*). In contrast to δTyr-228, where the level of labeling was increased in the presence of Carb or dTC, the level of labeling of δTyr-212 in the presence of Carb (or isoflurane) was reduced by <15%, but dTC inhibited labeling by 90%. Since there is no evidence that dTC binds near δTyr-212, we feel that it is unlikely that this inhibition results from a competitive interaction. dTC also reduced the total amount of [^{14}C]halothane incorporation in the δ subunit by ~25% and in αV8-18 by 50%, and we suspect that dTC acts as an aqueous scavenger of the reactive [^{14}C]halothane radical intermediate. However, further studies will be required to resolve this and to determine whether such a mechanism also contributes to the strong inhibition by dTC of [^{14}C]halothane labeling of γTyr-111, an amino acid near the entry of the ACh site (*49*) that is a dTC affinity determinant and is directly photolabeled by [^{3}H]dTC (*40*).

γTyr-105, which is exposed in the vestibule of the ion channel, was labeled in the absence or presence of Carb, dTC, or isoflurane, with the efficiency of labeling lowest in the presence of dTC. However, for γTyr-111 and γTyr-105, we do not have the data required from a parallel control labeling in the absence of added drugs to determine whether Carb or isoflurane is decreasing or increasing the labeling efficiency compared to the control.

[^{14}C]Halothane Photolabeling and Inhibition of nAChRs. Halothane inhibits the muscle type nAChR expressed on *Xenopus* oocytes with an IC_{50} of ~0.8 mM (*50*), and for *Torpedo* nAChR-rich membranes, it allosterically inhibits the binding of [^{3}H]phencyclidine with an IC_{50} of ~0.5 mM (*51*). We have shown that at these concentrations, [^{14}C]halothane is in contact with tyrosines in multiple regions of the nAChR extracellular domain and with δTyr-228 at the extracellular end of the δ subunit transmembrane domain. Although studies have not been carried out with halothane, for isoflurane, amino acids within the M2 ion channel domain have been identified as anesthetic potency determinants (*10*), which raises the possibility that volatile anesthetics, including halothane, bind directly within the lumen of the ion channel. Unfortunately, since there are no aromatics in the nAChR M2 segments, efficient halothane photoincorporation may not be possible, and halothane binding in the ion channel or other pharmacologically important sites lacking aromatic amino acids might be missed with this technique. However, photolabeling by [^{14}C]halothane did reveal labeling of δTyr-228 that is enhanced in the desensitized state, and since this

region in other nAChR subunits has been implicated in the gating mechanism (*44*, *45*), it is likely that halothane's interactions in this region contribute to its functional inhibition of the nAChR. The energetic contributions of δTyr-228 or other nearby amino acids to nAChR inhibition by halothane can be addressed by appropriate mutational analyses. In addition, further photolabeling studies will be required to determine whether there is state-dependent labeling of some of the labeled regions in the nAChR extracellular domain and to determine at the level of individual amino acids the labeling efficiencies as a function of [^{14}C]halothane concentration or the extent of inhibition by isoflurane or other general anesthetics.

REFERENCES

1. Franks, N. P., and Lieb, W. R. (1998) *Toxicol. Lett. 101*, 1−8.
2. Krasowski, M. D., and Harrison, N. L. (1999) *Cell. Mol. Life Sci. 55*, 1278−1303.
3. Yamakura, T., Bertaccini, E., Trudell, J. R., and Harris, R. A. (2001) *Annu. Rev. Pharmacol. Toxicol. 41*, 23−51.
4. Corringer, P.-J., Le Novere, N., and Changeux, J.-P. (2000) *Annu. Rev. Pharmacol. Toxicol. 40*, 431−458.
5. Karlin, A. (2002) *Nat. Rev. Neurosci. 3*, 102−114.
6. Mihic, S. J., Ye, Q., Wick, M. J., Koltchines, V. V., Krasowski, M. D., Finn, S. E., Mascia, M. P., Valenzuela, C. F., Hanson, K. K., Greenblatt, E. P., Harris, R. A., and Harrison, N. L. (1997) *Nature 389*, 385−389.
7. Jenkins, A., Greenblatt, E. P., Faulkner, H. J., Bertaccini, E., Light, A., Lin, A., Andreasen, A., Viner, A., Trudell, J. R., and Harrison, N. L. (2001) *J. Neurosci. 21*, RC136 (1−4).
8. Forman, S. A., Miller, K. W., and Yellen, G. (1995) *Mol. Pharmacol. 48*, 574−581.
9. Zhou, Q. L., Zhou, Q., and Forman, S. A. (2000) *Biochemistry 39*, 14920−14926.
10. Wenningmann, I., Barann, M., Vidal, A. M., and Dilger, J. P. (2001) *Mol. Pharmacol. 60*, 584−594.
11. Yamakura, T., Borghese, C., and Harris, R. A. (2000) *J. Biol. Chem. 275*, 40879−40886.
12. Downie, D. L., Vicenteagullo, F., Camposcaro, A., Bushell, T. J., Lieb, W. R., and Franks, N. P. (2002) *J. Biol. Chem. 277*, 10367−10373.
13. Kotzyba-Hibert, F., Kapfer, I., and Goeldner, M. (1995) *Angew. Chem., Int. Ed. 34*, 1296−1312.
14. Fleming, S. A. (1995) *Tetrahedron 51*, 12479−12520.
15. Chiara, D. C., Trinidad, J. C., Wang, D., Ziebell, M. R., Sullivan, D., and Cohen, J. B. (2003) *Biochemistry 42*, 271−283.
16. Pratt, M. B., Pedersen, S. E., and Cohen, J. B. (2000) *Biochemistry 39*, 11452−11462.
17. Pratt, M. B., Husain, S. S., Miller, K. W., and Cohen, J. B. (2000) *J. Biol. Chem. 275*, 29441−29451.
18. Arias, H. R., Kem, W. R., Trudell, J. R., and Blanton, M. P. (2002) *Int. Rev. Neurobiol. 54*, 1−50.
19. Bosterling, B., Trevor, A., and Trudell, J. R. (1982) *Anesthesiology 56*, 380−384.
20. Eckenhoff, R. G., and Shuman, H. (1993) *Anesthesiology 79*, 96−106.
21. Eckenhoff, R. G., and Johansson, J. S. (1997) *Pharmacol. Rev. 49*, 343−367.
22. Eckenhoff, R. G. (1996) *J. Biol. Chem. 271*, 15521−15526.
23. Eckenhoff, R. G., Pidikiti, R., and Reddy, K. S. (2001) *Biochemistry 40*, 10819−10824.
24. Ishizawa, Y., Pidikiti, R., Liebman, P. A., and Eckenhoff, R. G. (2002) *Mol. Pharmacol. 61*, 945−952.
25. Eckenhoff, R. G. (1996) *Proc. Natl. Acad. Sci. U.S.A. 93*, 2807−2810.
26. Middleton, R. E., and Cohen, J. B. (1991) *Biochemistry 30*, 6987−6997.
27. Blanton, M. P., and Cohen, J. B. (1992) *Biochemistry 31*, 3738−3750.
28. Pedersen, S. E., Dreyer, E. B., and Cohen, J. B. (1986) *J. Biol. Chem. 261*, 13735−13743.
29. Chiara, D. C., and Cohen, J. B. (1997) *J. Biol. Chem. 272*, 32940−32950.
30. White, B. H., and Cohen, J. B. (1988) *Biochemistry 27*, 8741−8751.
31. Brauer, A. W., Oman, C. L., and Margolies, M. N. (1984) *Anal. Biochem. 137*, 134−142.
32. Brejc, K., van Dijk, W. J., Klaassen, R., Schuurmans, M., van der Oost, J., Smit, A. B., and Sixma, T. K. (2001) *Nature 411*, 269−276.
33. Sullivan, D., Chiara, D. C., and Cohen, J. B. (2002) *Mol. Pharmacol. 61*, 463−472.
34. Miyazawa, A., Fujiyoshi, Y., and Unwin, N. (2003) *Nature 423*, 949−958.
35. Wang, D., Chiara, D. C., Xie, Y., and Cohen, J. B. (2000) *J. Biol. Chem. 275*, 28666−28674.
36. Gallagher, M. J., and Cohen, J. B. (1999) *Mol. Pharmacol. 56*, 300−307.
37. Chiara, D. C., Kloczewiak, M. A., Addona, G. H., Yu, J.-Y., Cohen, J. B., and Miller, K. W. (2001) *Biochemistry 40*, 296−304.
38. Blanton, M. P., and Cohen, J. B. (1994) *Biochemistry 33*, 2859−2872.
39. Cohen, J. B., Sharp, S. D., and Liu, W. S. (1991) *J. Biol. Chem. 266*, 23354−23364.
40. Chiara, D. C., Xie, Y., and Cohen, J. B. (1999) *Biochemistry 38*, 6689−6698.
41. Sine, S. M., Wang, H.-W., and Bren, N. (2002) *J. Biol. Chem. 277*, 29210−29223.
42. Cohen, J. B., and Strnad, N. P. (1987) in *Molecular Mechanisms of Desensitization to Signal Molecules* (Konijn, T., Ed.) pp 257−273, Springer-Verlag, New York.
43. Raines, D. E., and Zachariah, V. T. (2000) *Anesthesiology 92*, 775−785.
44. Akabas, M. H., and Karlin, A. (1995) *Biochemistry 34*, 12496−12500.
45. Zhang, H., and Karlin, A. (1997) *Biochemistry 36*, 15856−15864.
46. Yu, Y., Shi, L., and Karlin, A. (2003) *Proc. Natl. Acad. Sci. U.S.A. 100*, 3907−3912.
47. Cromer, B., Morton, C. J., and Parker, M. W. (2002) *Trends Biochem. Sci. 27*, 280−287.
48. Sawyer, G. W., Chiara, D. C., Olsen, R. W., and Cohen, J. B. (2002) *J. Biol. Chem. 277*, 50036−50045.
49. Sine, S. M. (2002) *J. Neurobiol. 53*, 431−446.
50. Violet, J. M., Downie, D. L., Nakisa, R. C., Lieb, W. R., and Franks, N. P. (1997) *Anesthesiology 86*, 866−874.
51. Lin, L., Koblin, D. D., and Wang, H. H. (1995) *Biochem. Pharmacol. 49*, 1085−1089.

BI0351561